PriMera Scientific Engineering
Volume 8 Issue 2 February 2026
ISSN: 2834-2550

PriMera Scientific Publications

Numerical Investigation of Passive Flow Control around a Cylinder with an Attached Splitter Plate

Type: Research Article
Received: December 19, 2025
Published: February 03, 2026

Citation:
Fazal Rahman. "Numerical Investigation of Passive Flow Control around a Cylinder with an Attached Splitter Plate". PriMera Scientific Engineering 8.2 (2026): 40-52.

Fazal Rahman*

Institute of Mathematical Sciences, Faculty of Science, Universiti Malaya, 50603 Kuala Lumpur, Malaysia

***Corresponding Author:** Fazal Rahman, Institute of Mathematical Sciences, Faculty of Science, Universiti Malaya, 50603 Kuala Lumpur, Malaysia.

Abstract

This research investigates the flow behavior around a cylinder with an attached splitter plate (L^*) using the lattice Boltzmann method (LBM). Although previous research has focused on flow around bluff bodies without L^*, this study examines the effects of L^* on flow control. The key parameters analyzed include L^* and the Reynolds number (Re). The vorticity contours, Drag coefficients C_D, lift coefficients C_L, and Strouhal numbers (St) are computed to elucidate the relationships L^* and Re. The results demonstrate that wake flow patterns, flow features, and force coefficients are strongly influenced by both L^* and Re. The flow is periodic at low Re, while it becomes irregular at high Re. The L^* effectively suppresses vortex shedding. Small L^* causes vortices to form near the cylinder, whereas large L^* stabilizes vortex shedding. Overall, L^* plays a great role in controlling vortex shedding, reducing drag, and regulating the lift force.

Keywords: Passive Method; Lattice Boltzmann Method; Vortex Shedding; Contours

Nomenclature

LBM	Lattice Boltzmann Method.
L^*	Splitter plate length.
Re	Reynold's number.
C_D	Drag coefficient.
C_L	Lift coefficient.
St	Strouhal number.
MEMS	Microelectromechanical systems.
CFD	Computational fluid dynamics.
FM	Fluid mechanics.
C_1	Cylinder 1.
C_{Dmean}	mean of C_D.
C_{Lrms}	root mean of C_L.
S_{tmean}	mean of St.

ρ	Density.
p	Pressure.
μ	Kinematic viscosity.
D_2	Two dimensional.
Q_9	Velocity directions.
e_i	Velocity set.
w_i	weighting coefficients.
U_∞	Inflow velocity.
L	Length.
D	size of cylinder.
C_{Lrms}	root mean of C_L.
S_{tmean}	mean of St.

Introduction

The suppression of fluid forces and flow control techniques have attracted a lot of attention recently due to their potential to improve the performance and efficiency of many engineering systems, buildings and structures, aeronautical engineering, etc., at large *Re*. On small *Re* applications can be are: cooling of electronic devices, microelectromechanical systems (MEMS) and computer equipment [1]. Passive flow control techniques among them present an appealing option, since they do not require active control mechanisms or external energy input. Reduction of the fluid forces acting on a cylinder with an attached splitter plate at different *Re* by the passive method has not yet been studied extensively. In this research, flow around a cylinders with attached splitter plates can be examined using the lattice-Boltzmann method (LBM). LBM is a recent advance in computational fluid dynamics (CFD). While standard CFD methods discretize and solve the macroscopic equations of fluid mechanics (FM) directly, the LB approach solves a discrete kinetic equation that replicates the FM equations in the macroscopic limit.

The cylindrical structure is among the most often used engineering structures, such as chimneys, piers, offshore platform struts, condenser pipes, and many others used for flow control purposes [2]. Flow across a cylinder is practically related to numerous technical applications, such as large buildings, bridges, and vertical columns of a sea platform placed side-by-side [3], tandem [4], or both [5]. An efficient flow control could conserve energy, improve propulsion efficiency, and reduce body vibration. Generally speaking, there are two ways to actively [6] or passively [7, 8] manage a flow field and aerodynamic forces to achieve the desired technological change based on their significance. Numerous strategies have been proposed to improve lift, reduce drag, delay transitions, and increase in the event of turbulence. Compared to active control, passive control is simpler and easier. LBM can simulate a variety of flows, including multiphase [9, 10], multicomponent [11-13], complex fluid flows [14], flows in intricate geometries, such as porous media [15] and turbulent fluxes [16].

[17] used finite volume approach was to numerically evaluate how a flat plate affected the fluid force over a square cylinder in a cross flow. The output reveals that the control plate has a great effect on drag, lift and vorticity contours. [18, 19] used splitter plate in different arrangements and they reach on the conclusion that large splitter plate greatly control vortex shedding, drag, lift and strouhal number. Using L^* at different *Re*′s is the main novelty of this work. Scientist Rahman [20] investigated the effects of splitter plate length, gap spacing between three cylinders, and Reynolds's number on flow past three cylinders arranged in a triangular configuration (two downstream cylinders and one upstream cylinder with attached splitter plates). The study found that all three parameters significantly influence the flow behavior, drag reduction, and lift control.

Material and Method

Problem description

The geometry of the chosen problem shown in Fig. 1 represents the 2D computation region, where a cylinder is fixed and remain

motionless, designated as cylinders C_1. The goal of this research is to control the flow when a cylinders is placed in a chennel by the passive method. Passive methods in flow control refer to techniques that alter the flow characteristics without requiring external energy input. The study is carried out for two different *Re*′s with *L** ranging from 0 to 5. Periodic boundary conditions are utilized at the inlet and outlet of the channel, while no-slip boundary conditions are employed on the surface of the cylinders. The front position of the domain includes the uniform inflow condition ($u = U_{max}$, $v = 0$). On the surface of the cylinder no slip boundary condition using a bouncing-back scheme are adopted.

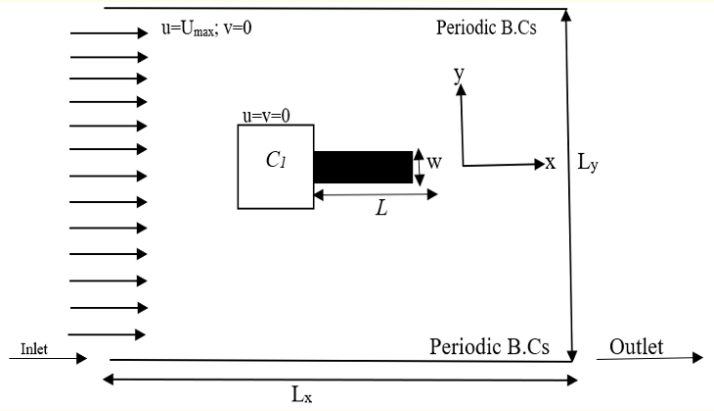

Figure 1: Geometry of problem.

Governing equations

The flow around a cylinder with a splitter plate attached is investigated numerically, taking into account the coupling, the bluff body structure and the flow field. The flow field model takes into account the two-dimensional Newtonian, laminar, and incompressible fluid. The Navier-Stokes equation as the governing equation.

$$\nabla . u = 0 \tag{1}$$

$$\rho(\frac{\partial u}{\partial t} + u\nabla u) + \nabla p = \mu \Delta u + f \tag{2}$$

Where ρ is the density, p is the pressure, u is the velocity, μ is the kinematic viscosity and f is the force on fluid.

Numerical Method

The LBM equation can be used to express equations (1) and (2).

$$f_i(x + e_i\Delta t, y + e_i\Delta t, t + \Delta t) - f_i(x, y, t) = \Omega(f) \tag{3}$$

Where Ω (f) is found by Bhatnagar-Gross-Krook (BGK) which is:

$$\Omega(f) = \frac{-1}{\tau}(f - f^0) \tag{4}$$

The Boltzmann equation with BGK collision operator is:

$$f_i(x + e_i\Delta t, y + e_i\Delta t, t + \Delta t) - f_i(x, y, t) = \frac{-1}{\tau}[f_i(x, y, t) - f_i^0(x, y, t)] \tag{5}$$

Equilibrium distribution function is:

$$f_i^0(x,t) = w_i\rho(x,t)[1 + \frac{eiu}{c_s^2} + \frac{1}{2}\frac{(e_i.u)^2}{c_s^4} - \frac{1}{2}\frac{u^2}{c_s^2}] \tag{6}$$

The fluid density and velocity can be find are defined as:

$$\rho(x, y, t) = \sum f_i(x, y, t) \tag{7}$$

$$u(x, y, t) = \frac{1}{\rho}\sum e_i f_i(x, y, t) \tag{8}$$

Here in Eqn. (3) to (8), f_i is the particle distribution function for velocity component i, e_i is the velocity of particle, Δt is time step, τ is relaxation time, and f_i^0 is equilibrium distribution function, w_i is weighting coefficient which has different values for different system, and c_s is speed of sound.

The D_2Q_9 model's bounce-back boundary conditions were employed in this investigation.

e_i are the velocity and Fig. 2 represents 9 different velocities for the D_2Q_9 model.

$$e_i = \begin{cases} c(0,0) \quad \text{for} \quad i = 0 \\ c(cos(\frac{\pi}{2}(i-1)), sin(\frac{\pi}{2}(i-1))), \quad \text{for} \quad i = 1,2,3,4 \\ \sqrt{2}c(cos(\frac{\pi}{2}(i-\frac{9}{2})), sin(\frac{\pi}{2}(i-\frac{9}{2}))), \quad \text{for} \quad i = 5,6,7,8 \end{cases} \tag{9}$$

For the D_2Q_9 model, the c_s value is $\frac{1}{\sqrt{3}}$. The w_i values for D_2Q_9 are:

$$w_i = \begin{cases} \frac{4}{9} \quad \text{for} \quad i = 0 \\ \frac{1}{9} \quad \text{for} \quad i = 1,2,3,4 \\ \frac{1}{36} \quad \text{for} \quad i = 5,6,7,8 \end{cases} \tag{10}$$

The dimensionless Reynolds number (*Re*) is determined by

$$Re = \frac{U_\infty L}{v} \tag{11}$$

where U_∞ is the inlet velocity, L is the characteristic length and v is the kinematic viscosity. Drag coefficients C_D can be determined by

$$C_D = \frac{2F_d}{\rho U_\infty^2 D} \tag{12}$$

Here F_d is the drag force and D is the size of the cylinder. Lift coefficients C_L can be determined as

$$C_L = \frac{2F_l}{\rho U_\infty^2 D} \tag{13}$$

Here F_l is lift force. The *St* can be determined as

$$St = \frac{f_s D}{U_\infty} \tag{14}$$

Where f_S is the frequency of vortex shedding. C_{Drms} and C_{Lrms} can be computed by these relations

$$C_{Drms} = \sqrt{\sum_{t=1}^{n}[C_D(t) - C_{Dmean}]^2/n} \tag{15}$$

$$C_{Lrms} = \sqrt{\sum_{t=1}^{n}[C_L(t) - C_{Lmean}]^2/n} \tag{16}$$

Where *n* is how many time steps there are.

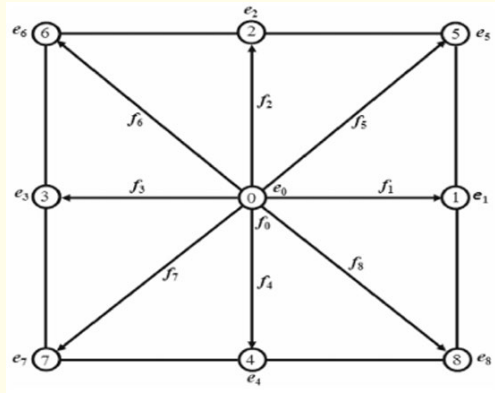

Figure 2: D_2Q_9 model.

Computation Domain

Fig. 1. shows a schematic illustration of the suggested problem. In an unconfined computational domain, one obstacles of dimension "D" are inserted to a cross-flow with a continuous inlet velocity (U_∞). The subscript ∞ in U_∞ denote quantities that are distant from the cylinders. Downstream attaches a stiff, thin splitter plates to the cylinders, each measuring *L** in length and *W* in thickness. The *L** thickness is fixed at $w = 0.1D$. In this study, the thin, stiff plate is referred to as splitter plates. To make the study of the chosen problem computationally viable, the borders of the computational domain are positioned effectively far from the cylinders and bounce back scheme is adopted. The two-dimensional flow is represented by a Cartesian coordinate system (x and y), where the cross-sectional and streamwise directions are represented by the y-axis and the x-axis, respectively. The grid points in the transverse and streamwise directions is denoted by L_y and L_x, respectively. L_u is the upstream distance from the inlet position to the front surface of the upstream cylinders. The downstream distance from the downstream splitter plate rear surface to the computational domain's exit is denoted by L_d. This study uses $L_u = 10D$ and $L_d = 25D$ for calculations. By altering the values of *L**, the grid points in the horizontal and upward directions can be changed. The complete details of our codes are available in our previously published papers [21-23].

Code Validation

Table 1 compares this study with previous research on a square cylinder at *Re* = 100.

Table 2 shows the effect of the *L** on C_{Dmean}, C_{Lrms}, and *St* at two *Re*'s. For *Re* = 100, the values of C_{Dmean}, C_{Lrms}, and *St* are high when no *L** is attached (*L** = 0). When the *L** is attached, the value of C_{Dmean} decreases; however, a further increase in *L** does not produce significant changes. In the case of C_{Lrms}, the value reduces with increase in *L** and becomes zero for *L** = 4 and 5. The *St* is not significantly affected by small values of *L**, but for larger values of *L**, it decreases to zero. Thus, *St* is more strongly affected by large *L**. For *Re* = 200, the effect of *L** is more pronounced than for *Re* = 100. The values are again high when no *L** is attached and decrease when the *L** is added. The reduction in C_{Dmean} is 20.09 % for *L** = 1, whereas for *Re* = 100 it was 16.28%. For *L** = 2, the value first increases and then decreases. This behavior occurs because the *L** causes flow reattachment on the cylinder, which increases the value; this effect is not observed for *Re* = 100. For larger values of *L**, C_{Dmean} decreases again. The value of C_{Lrms} also decreases with increasing *L**, but it does not reach zero at *Re* = 200. A similar trend is observed for the *St*.

References	C_D	C_L	***St***	***Method***
Sarwar et al. (2023)	1.38	-	0.144	LBM
Wei et al. (2023)	1.46	0.184	0.144	IBLBM
Sen et al. (2015)	1.52	0.192	0.142	FEM
Berrone et al. (2009)	1.46	-	0.144	FVM
Present work	1.3729	0.168	0.145	LBM

Table 1: Comparison with previous studies.

Re	***L****	C_{Dmean}	***% Reduction in*** C_{Dmean}	C_{Lrms}	***% Reduction in*** C_{Lrms}	***St***	***% Reduction in St***
100	0	1.3729	0	0.1688	0	0.1448	0
	1	1.2101	16.28	0.0642	10.46	0.1302	1.46
	2	1.1921	1.8	0.0282	3.6	0.1302	0
	3	1.1752	1.69	0.0016	2.66	0.1167	1.35
	4	1.1798	0.46	0	0.16	0	11.67
	5	1.1811	0.13	0	0	0	0
200	0	1.3930	0	0.3787	0	0.1494	0
	1	1.1921	20.09	0.1977	18.1	0.0972	5.22
	2	1.2429	5.08	0.1947	0.3	0.1671	6.99
	3	1.2191	2.38	0.2315	3.68	0.1448	2.23
	4	1.1948	2.43	0.2308	0.07	0.1179	2.69
	5	1.1779	1.69	0.2066	2.42	0.0972	2.07

Table 2: Splitter plate effects on three parameters.

Fig. 3 shows the variation of C_{Dmean}, C_{Lrms}, and *St* with *L** at two different *Re*'s. The values are higher for *Re* = 200 than for *Re* = 100. The values of C_{Dmean} and C_{Lrms} are high when no *L** is attached (*L** = 0) but decrease significantly when the *L** is added. However, a further increase in *L** produces only a minimal effect on C_{Dmean} and C_{Lrms}.

The value of C_{Lrms} becomes zero for *L** = 4 and 5 at *Re* = 100, whereas it does not reach zero at *Re* = 200, indicating that flow disturbances still exist even at *L** = 5. The *St* at *Re* = 100 shows little change for small values of *L** but decreases to zero for *L** = 4 and 5. In contrast, for *Re* = 200, the effect on *St* is small and it does not reach zero, indicating the presence of oscillations.

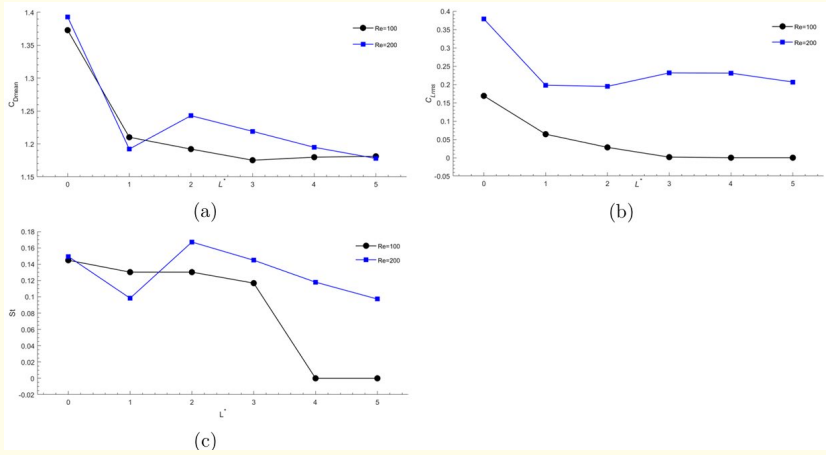

Figure 3: Splitter plate effect with two Reynolds numbers on: (a) C_{Dmean}, (b) C_{Lrms} and (c) *St*.

Results and Discussions

The investigations are computed for 6 *L** lengths starts from zero and incremented by 1. Two *Re*′s are taken into account. Results with significant affects are discussed here to avoid repetition.

Effect of L on Re=100*

For *Re* = 100, three *L** lengths are considered. Vorticity contours, streamlines, C_D, C_L and the *St* are computed to evaluate the effect of *L** length on the flow behavior. Vorticity contours for *Re* = 100 and three different values of *L** are presented in Fig. 4. For *L** = 1, vortices form near the cylinder, more flow reattaches on the cylinder, and the vortices are periodic. For *L** = 3, the vortices become stronger and more stable, and vortex deflection starts farther away from the cylinder. Since *L** is still relatively small, some deflection is observed. In the case of *L** = 5, a fully developed flow pattern is formed. The vortices are stable, and no deflection is observed. This flow pattern is referred to as a fully developed flow pattern.

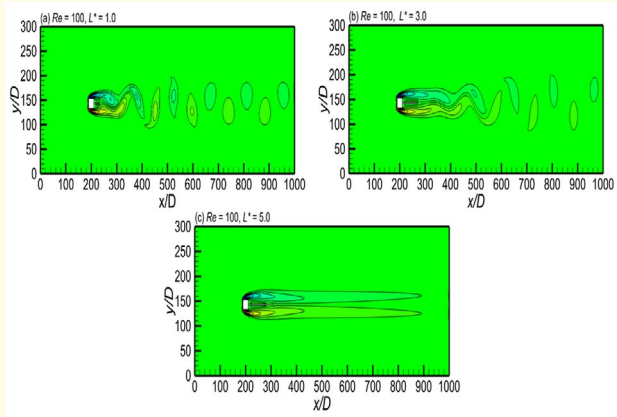

Figure 4: Vorticity contours on *Re* = 100.

The corresponding streamlines for the vorticity contours are shown in Fig. 5. For small values of L^*, two eddies are formed, one of which appears in front of the L^* and has a strong effect on the flow behavior. The deflection of the streamlines indicates the presence of flow disturbances. For $L^* = 3$, the streamlines are better organized compared to $L^* = 1$. No eddy is formed in front of the L^*; however, side eddies still produce some disturbances. For $L^* = 5$, two eddies are formed along the sides of the L^*, but their effect diminishes due to the larger L^*. No eddy is formed in front, and the streamlines show no deflection. The fully developed flow pattern observed in the vorticity contours is also evident in the streamlines.

The C_D and C_L corresponding to the vorticity contours and streamlines are shown in Fig. 6. Both C_D and C_L are periodic due to $Re = 100$. The value of C_D is maximum for $L^* = 1$, and strong oscillations are observed. Similarly, C_L has higher values and larger oscillations for $L^* = 1$. For $L^* = 3$, the values of C_D and C_L decrease, and the oscillations are reduced due to the more stable vortices observed in Fig. 4. However, the oscillations in C_L increase with time as vortex deflection begins farther from the cylinder. For $L^* = 5$, C_D reaches its minimum value and shows no oscillations because of the stable and fully developed flow pattern seen in Fig. 4. The value of C_L becomes zero, indicating a stable flow with no disturbances.

The power spectra of the St are shown in Fig. 7. The power spectrum of St is high for $L^* = 1$ due to strong oscillations in the flow. The power spectrum decreases for $L^* = 3$ because the vortices become more stable and the oscillations are weaker. In the case of $L^* = 5$, the power spectrum vanishes and approaches zero, indicating stable vortices and the absence of oscillations.

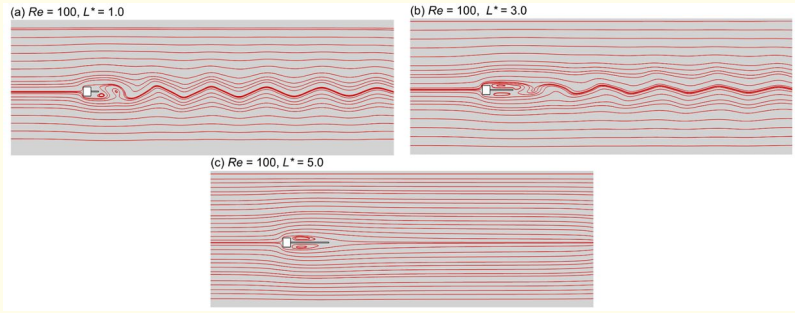

Figure 5: Streamlines on $Re = 100$.

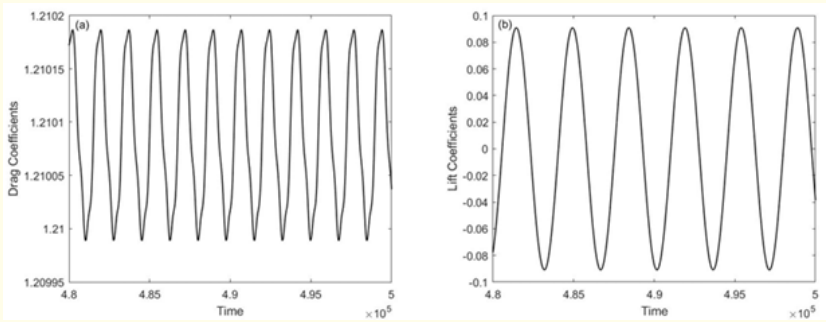

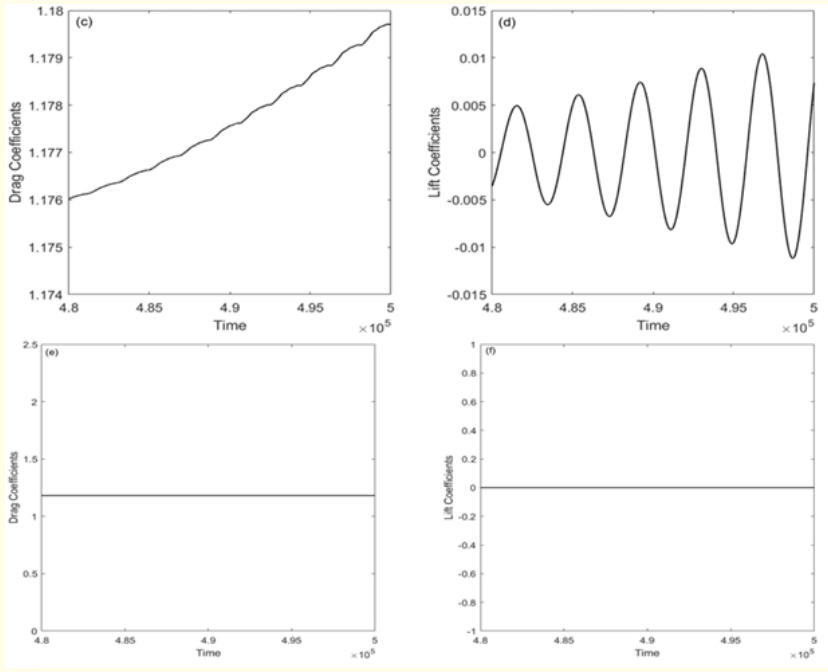

Figure 6: Drag and lirft coefficients on *Re* = 100: (a, b) *L** = 1 (c, d) *L** = 3, (e, f) *L** =5.

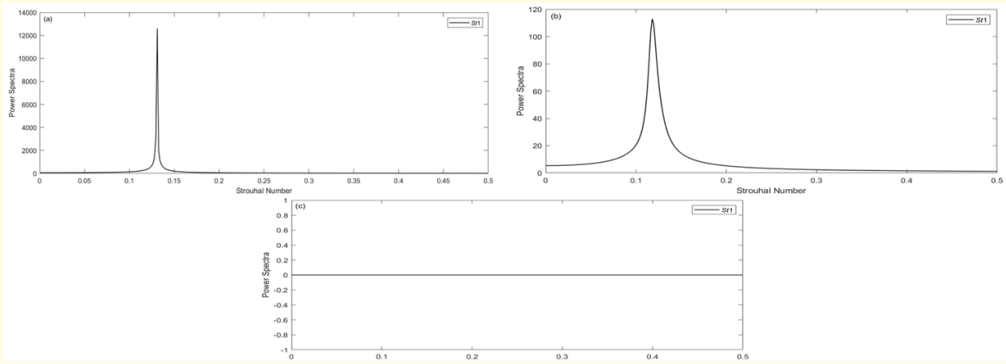

Figure 7: Power spectra of strouhal number on *Re* = 100: (a) *L** = 1 (b) *L** = 3, (c) *L** = 5.

Effect of L on Re=200*

The effect of the *Re* = 200 on the vorticity contours at different values of *L** is shown in Fig. 8. When *L** = 1, more flow reattaches on the cylinder, and the vortex shedding is not periodic. The vortex deflection is larger compared to the case of *Re* = 100. For *L** = 3, the vortices become periodic; however, they do not strengthen with increasing *L** at *Re* = 200. More flow reattach on cylinder compare to *L** = 1 because L* suppresses vortices. In contrast, for Re = 100, stable and stronger vortices are observed, which is not the case for *Re* = 200. For *L** = 5, the vortices become stronger and vortex deflection starts farther from the cylinder, whereas for *Re* = 100, a fully developed flow pattern is observed. Overall, for small values of *L**, the vortices are not periodic, while for larger values of *L**, periodicity

is regained.

The streamlines corresponding to the vorticity contours are shown in Fig. 9. For $L^* = 1$, a large eddy forms in front of the L^*, strongly affecting the flow pattern and causing significant disturbances. Oscillations and irregularities are clearly visible in Fig. 9(a). For $L^* = 3$, a small eddy forms below the L^*, reducing its effect on the flow. The flow regains periodicity, and although oscillations are present, the flow pattern is improved compared to Fig. 9(a). For $L^* = 5$, two eddies form above and below the L^*, but their effect persists due to $Re = 200$. In contrast, for $Re = 100$, smooth streamlines were observed.

The C_D and C_L corresponding to the vorticity contours are shown in Fig. 10. For $L^* = 1$, the oscillations are small at Re = 200 because less flow reattaches on the cylinder. Non-periodic behavior is observed in both C_D and C_L, which vary differently over time. For $L^* = 3$, the oscillations increase compared to $L^* = 1$ because the L^* suppresses vortices, causing more flow to reattach on the cylinder. Periodicity is regained, and both C_D and C_L show periodic behavior. The oscillations are larger than for $Re = 100$, where they are reduced. For $L^* = 5$, the values of C_D and C_L are minimum and periodic, but oscillations are still present due to $Re = 200$. In contrast, for $Re = 100$, C_D shows no oscillation and C_L is zero at $L^* = 5$.

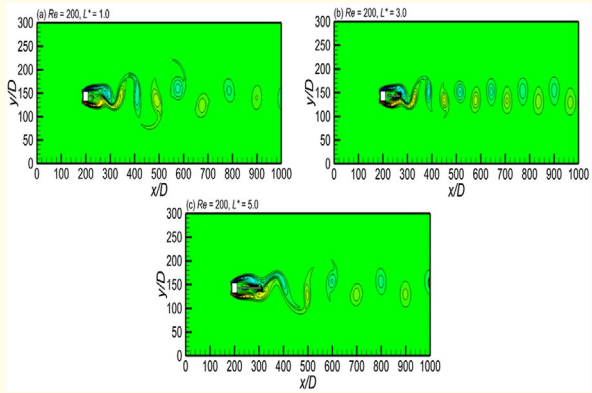

Figure 8: Vorticity contours on $Re = 200$.

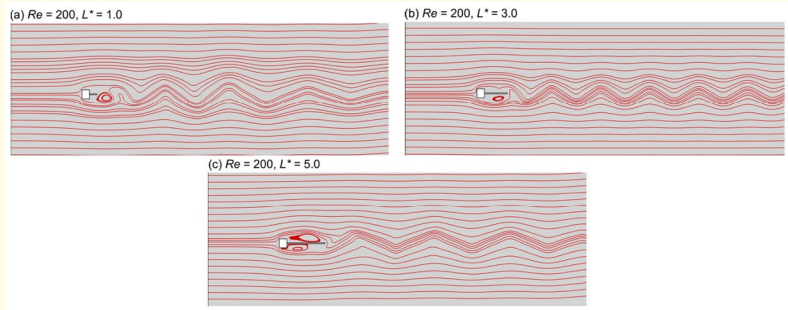

Figure 9: Streamlines on $Re = 200$.

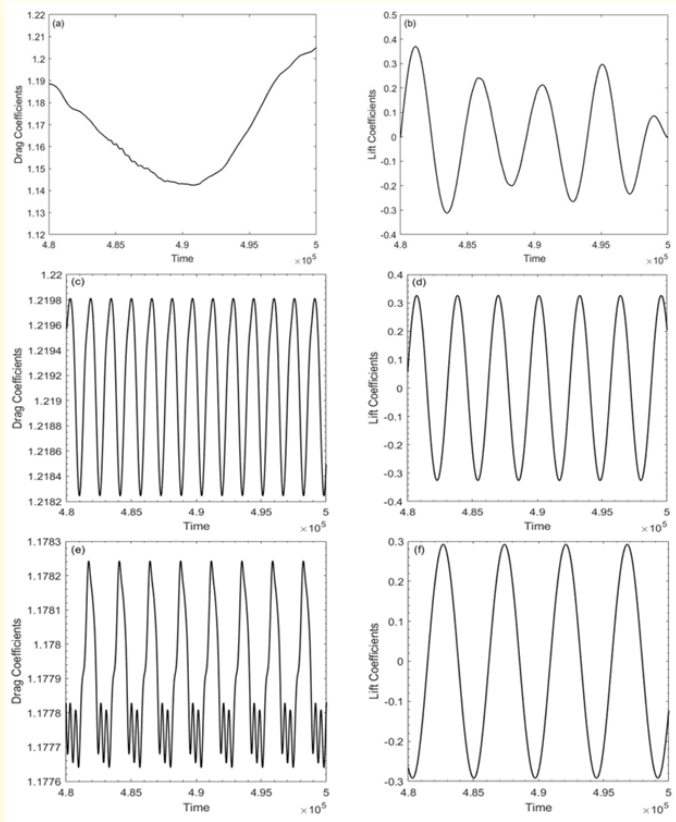

Figure 10: Drag and lirft coefficients on *Re* = 200: (a, b) *L** = 1 (c, d) *L** = 3, (e, f) *L** = 5.

The power spectra of the *St* corresponding to the vorticity contours are shown in Fig. 11. For *L** = 1, the power spectrum is lower than for *L** = 3, but a noisy structure is observed. This is due to small *L**, which causes stronger disturbances and vortex deflection, resulting in the noise. The power spectrum is maximum for *L** = 3 because more flow reattaches to the cylinder as the *L** suppresses vortices. For *L** = 5, the power spectrum decreases compared to *L** = 3 due to the formation of stable vortices. The power spectrum is still non-zero at *Re* = 200 because of the remaining disturbances, whereas for *Re* = 100, the power spectrum was zero.

Conclusion

The flow past to a cylinder with attached splitter plates was numerically investigated using the LBM to address fluid-structure interactions. The study focused on the effects of splitter plate length (*L**) and Reynolds number (*Re*) on fluid dynamics, including wake structures, streamlines, C_D, C_L, and the *St*.

- The *Re* has a significant impact on C_D, C_L, and *St*, causing their values to increase or decrease.
- The *L** strongly affects vortex suppression, C_L, and *St*, helping to stabilize the flow pattern.
- At low *Re*, the flow is periodic, while at high *Re*, the flow becomes non-periodic.
- For small *L**, vortices exhibit more deflection, whereas for large *L**, the vortices are elongated.
- At *Re* = 200, small *L** results in lower C_L and *St* values, while large *L** leads to higher values.

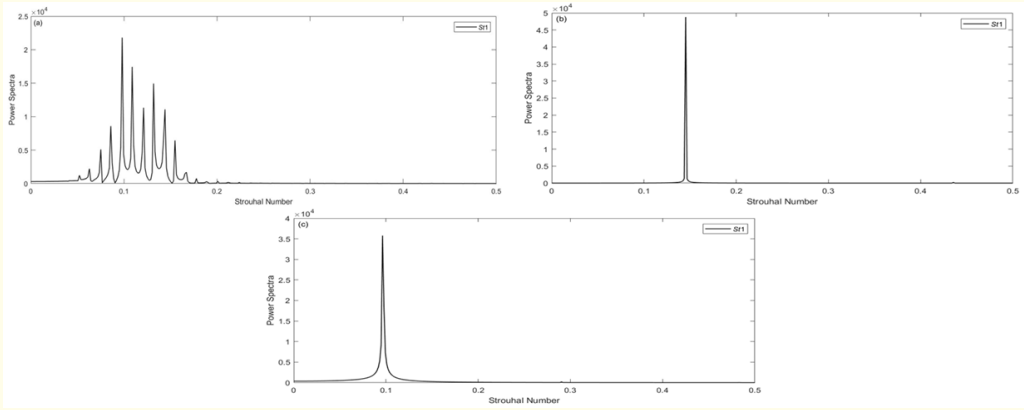

Figure 11: Power spectra of strouhal number on *Re* = 200: (a) *L** = 1 (b) *L** = 3, (c) *L** = 5.

References

1. Islam ZU, Islam SU and Zhou CY. "Flow control around two side-by-side square cylinders using dual splitter plates". J Braz. Soc. Mech. Sci. Eng (2021).
2. Rahman H., et al. "Numerical simulations of flow characteristics of two side-by-side square cylinders with connected splitters". Comp. Part. Mech (2023).
3. Islam SU, Rahman H and Zhou CY. "Comparison of wake structures and force measurements behind three side-by-side cylinders". J Braz Soc Mech Sci Eng (2014a).
4. Islam SU., et al. "Numerical investigation of wake modes for flow past three tandem cylinders using the multi-relaxation-time lattice Boltzmann method for different gap spacings". J. Braz. Soc. Mech. Sci. Eng (2014b).
5. Lima SA, Silva A and Silveira NA. "Numerical simulation of two-dimensional complex flows around bluff bodies using the immersed boundary method". J. Braz. Soc. Mech. Sci. Eng (2007).
6. Fujisawa N., et al. "Computational and experimental study on flow around a rotationally oscillating circular cylinder in a uniform flow". J Wind Eng Ind Aerodynamic (2005).
7. Islam SU., et al. "Suppression of fluid force on flow past a square cylinder with a detached flat plate at low Reynolds number for various spacing ratios". J. Mech. Sci. Technol (2014).
8. Hwang Llim HC and Lee SJ. "Flow control of a circular cylinder with O-rings". J. Fluid Dynamics Research (2004).
9. Gunstensen AK, Rothman DH and S Zaleski. "Lattice Boltzmann model of immiscible fluids". J. Physical Review A (1991).
10. Grunau D, Chen S and Eggert K. "A Lattice Boltzmann model for multiphase fluid flows". J. Physical Fluid A (1993).
11. Chen H, Chen S and WH Matthaeus. "Recovery of the Navier-Stokes equation using a Lattice Boltzmann method". Physical Review A (1983).
12. Qian YH, Dhumieres D and Lallemand P. "Lattice BGK model for the Navier stokes equations". J. Europhysics Letters (1992).
13. Chen S and Doolen GD. "Lattice Boltzmann method for fuid flows". J. Annual Review of Fluid Mechanics (1998).
14. Shaik Feroz. "Lattice Boltzmann Method for Fluid Flow". J. Fluid Mech. Open Acc (2021).
15. Ehsan F., et al. "Lattice Boltzmann methods in porous media simulations: From laminar to turbulent flow". J. Computers and Fluids (2016).
16. Pavel E, Vladimr F and Radek F. "Cumulant lattice Boltzmann simulations of turbulent flow above rough surfaces". Computers and Mathematics with Applications (2021).
17. Zhou CY., et al. "Numerical Study of Fluid Force Reduction on a Square Cylinder Using a Control Plate". Journal of the Brazilian

Society of Mechanical Sciences and Engineering (2009).

18. Rahman F and Islam SU. Passive Flow Control in Triangular Arrangement of Cylinders: Role of Reynold's Number, Role of Gap Spacing, Role of Splitter plate (2025).
19. Islam SU., et al. "Suppression of fluid force on flow past a square cylinder with a detached flat plate at low Reynolds number for various spacing ratios". J Mech Sci Technol 28, (2014): 4969-4978.
20. Islam SU., et al. "Lattice Boltzmann Study of Wake Structure and Force Statistics for Various Gap Spacings Between a Square Cylinder with a Detached Flat Plate". Arab J Sci Eng 40, (2015): 2169-2182.
21. Abbasi WS., et al. "Numerical Investigation of Fluid-Solid Interaction for Flow Around Three Square Cylinders". AIP Advances 1 (2018).
22. Abbasi WS and Islam SU. "Transition from steady to unsteady state flow around two inline cylinders under the effect of Reynolds numbers". J Braz. Soc. Mech. Sci (2018).
23. Rahman H., et al. "Flow structure mechanism around three rectangular bodies using the Lattice Boltzmann method". Ocean Engineering (2020).
24. Wei LW., et al. "Spanwise wake structures of a circular cylinder and two circular cylinders in tandem (2023).